Supporting Information

Nickel Tungstate-Graphene Nanocomposite for Simultaneous Electrochemical Detection of Heavy Metal Ions with Application to Complex Aqueous Media

Rudra Kumar,[a#] Thiruvelu Bhuvana,[b#*] and Ashutosh Sharma[a*]

[a]Department of Chemical Engineering, Indian Institute of Technology, Kanpur 208016, India.

[b]Department of Mechanical Engineering, Indian Institute of Technology, Kanpur 208016, India

E-mail: bhuvana@iitk.ac.in; ashutos@iitk.ac.in

[#] contributed equally

XPS

X-ray photoelectron spectroscopy (XPS, PHI 5000 Versa Prob II, FEI, USA) were measured in the range from 0-1100 eV. The chemical bonding and composition were determined by XPS and the survey scan of RGO/$NiWO_4$ nanocomposite is shown in **Figure S1a**. The peak identified at 36, 68, 112, 259, 284, 426, 496, 531 and 857 eV corresponded to W (4f), Ni (3p), Ni (3s), W (4d), C (1s), W ($4p_{3/2}$), W ($4p_{1/2}$), O (1s), Ni(2p) eV respectively. The high resolution of Ni 2p spectra shown is in the **Figure S1b**. The peak obtained at 856.1eV of Ni $2p_{3/2}$ confirmed the presence of Ni ions in divalent oxidation state.[1] The peak of Ni $2p_{1/2}$ core level was identified at 873.7 eV. Further, the satellite peak at 863.14 eV corresponded to Ni $2p_{3/2}$. The energy difference of 17.27 eV in between of Ni $2p_{3/2}$ and Ni $2p_{1/2}$ core levels confirmed the Ni^{2+} oxidation state. Furthermore, the W $4f_{7/2}$ peak appearing at 35.8 eV and combining with the Ni $2p_{3/2}$ peak at 856.1 eV together suggested the formation of $NiWO_4$ binary metal oxide.[2] **Figure S1c** showed the high-resolution XPS spectra of W 4f. The peak obtained at 35.8 and 38 eV corresponded to W$4f_{7/2}$ and W$4f_{5/2}$ respectively. The deconvoluted

O 1s core level spectrum (**Figure S1d**) showed two peaks at 531.4 eV and 533.6 eV, respectively, attributed to the oxygen species in nickel spinel oxide and C=O.[3] The de-convoluted C 1s core level spectrum (**Figure S1e)** showed four binding energies at 284.8 eV, 285.8 eV, 288.4 eV, and 291.0 eV, corresponding to sp^2 and sp^3 hybridized carbon, C−O, and O=C−O functional groups, respectively.[3]

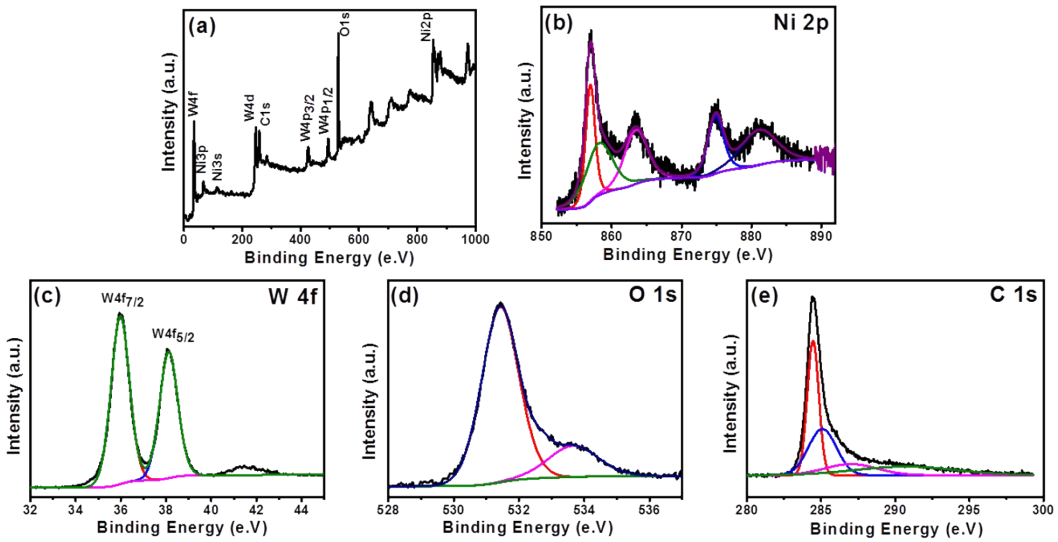

Figure S1: XPS of RGO/$NiWO_4$ nanocomposite (a) survey spectrum, (b) Ni 2p, (c) W 4f, (d) O 1s and (e) C 1s.

Energy dispersive X-ray spectroscopy (EDX) and elemental mapping of RGO/$NiWO_4$ nanocomposite are shown in **Figure S2** which confirmed the homogeneous distribution of C, O, Ni, and W elements.

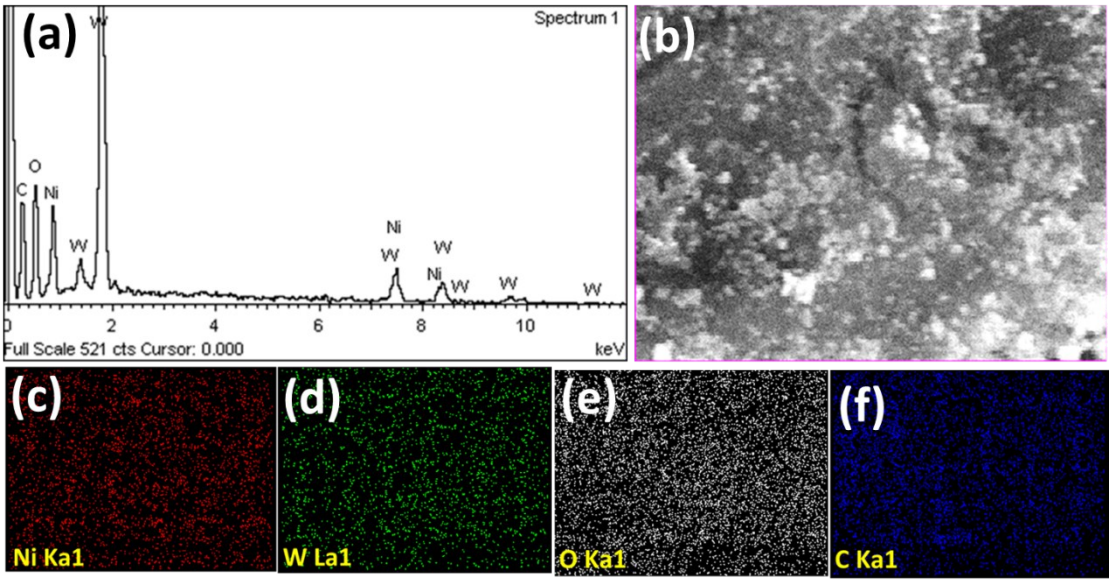

Figure S2: (a) EDX of RGO/$NiWO_4$ nanocomposite, (b) SEM and elemental mapping of Ni, W, O and C (c-f) respectively.

BET

The specific surface area and total pore volume of $NiWO_4$ and RGO/$NiWO_4$ nanocomposite were measured by N_2 adsorption/desorption isotherm using Autosorb iQ-BET, Quantachrome Instruments, USA. **Figure S3a and S3b** showed the nitrogen adsorption desorption isotherm. The Brunauer–Emmett–Teller (BET) surface area of $NiWO_4$ and RGO/$NiWO_4$ nanocomposite were 18 $m^2\ g^{-1}$ and 56 $m^2\ g^{-1}$, respectively. The total pore volume of $NiWO_4$ and RGO/$NiWO_4$ nanocomposite was 0.016 $cm^3\ g^{-1}$ and 0.15 $cm^3\ g^{-1}$, respectively. The increase in surface area, as well as pore volume of RGO/NiWO4 nanocomposite, is due to the wrapping of high surface area graphene sheets into $NiWO_4$ nanoparticles, which also prevented the restacking of graphene sheets. The pore size distribution was determined by Barrett–Joyner–Halenda (BJH) method. Inset of **Figure S3(a-b)** shows the pore size distribution of $NiWO_4$ and RGO/$NiWO_4$ nanocomposite, confirmed the mesoporous nature. The pore size of 3.82 nm and 9.54 nm were obtained for $NiWO_4$ NPs and RGO/$NiWO_4$, respectively.

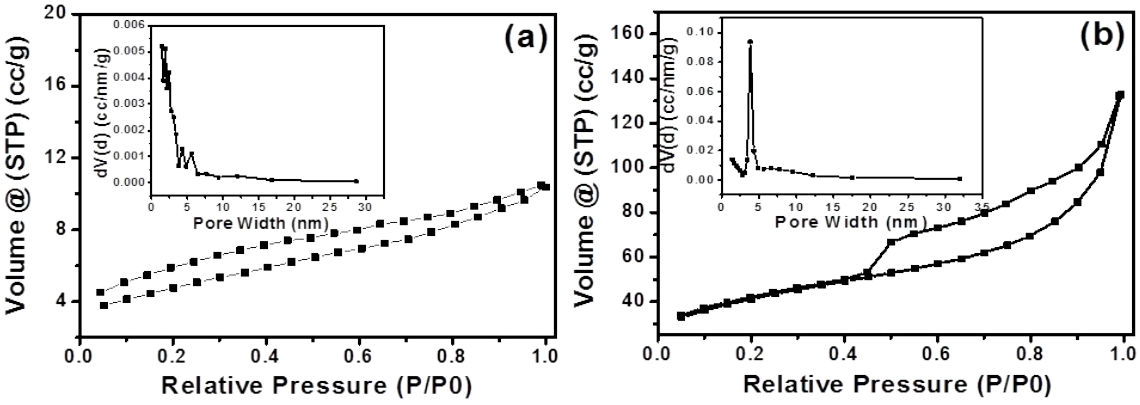

Figure S3: N_2 Adsorption desorption spectra of (a) $NiWO_4$ NPs and (b) RGO/$NiWO_4$ nanocomposite and inset showing pore size distribution.

Table S1: Comparative study of the electrochemical detection of Cd(II), Pb(II), Cu(II), Hg(II) ions performed for RGO/$NiWO_4$ nanocomposite electrode.

Type	Analyte	Sensitivity ($mA.\mu M^{-1}.cm^{-2}$)	LOD (10^{-10} M)	Correlation Coefficient	Intercept
Individual Analysis	Cd(II)	0.1145	4.75	0.9978	0.5419
	Pb(II)	0.0341	3.79	0.9910	5.327
	Cu(II)	0.0401	4.41	0.9986	1.616
	Hg(II)	0.0683	2.83	0.9968	1.0549
Simultaneous Analysis	Cu(II)	0.1173	1.12	0.9967	0.8899
	Hg(II)	0.1245	1.20	0.971	0.9794
Simultaneous Analysis	Cd(II)	0.0622	0.12	0.9905	0.7597
	Cu(II)	0.1411	1.16	0.9954	1.6348
	Hg(II)	0.1651	1.36	0.9975	1.6368
Simultaneous Analysis	Pb(II)	0.08571	2.04	0.9952	3.168
	Cu(II)	0.07432	1.77	0.9983	4.304
	Hg(II)	0.08094	1.92	0.9962	3.742
Simultaneous Analysis	Cd(II)	0.00998	2.05	0.9883	0.0814
	Pb(II)	0.0098	1.95	0.9943	0.0202
	Cu(II)	0.01465	3.42	0.9958	0.088
	Hg(II)	0.01401	3.41	0.9813	0.0952
Carbonated Drink	Cd(II)	0.0008	1.11	0.9965	0.0148
	Pb(II)	0.0147	2.04	0.9999	0.0812
	Cu(II)	0.0202	2.80	0.9883	0.1132
	Hg(II)	0.2192	3.05	0.9929	0.1193

Milk	Cd(II)	0.0027	3.83	0.9993	0.00673
	Pb(II)	0.0149	2.09	0.9984	0.00581
	Cu(II)	0.0125	1.74	0.9983	0.00547
	Hg(II)	0.00671	9.34	0.9927	0.00671
Orange Juice	Cd(II)	0.0211	2.72	0.9905	0.0299
	Pb(II)	0.01634	2.26	0.9999	0.0898
	Cu(II)	0.1468	2.04	0.9870	0.022
	Hg(II)	0.02073	2.88	0.9907	0.0089

Table S2. Comparison of LOD from literature for individual and simultaneous detection

Type	Analyte	LOD (10^{-10} M)	Ref
Individual Analysis	Cd(II)	4.75	Present
	Pb(II)	3.79	
	Cu(II)	4.41	
	Hg(II)	2.83	
Simultaneous Analysis	Cd(II)	2.05	
	Pb(II)	1.95	
	Cu(II)	3.42	
	Hg(II)	3.41	
Individual Analysis	Cd(II)	3.8	4
	Pb(II)	2.5	
	Cu(II)	13.0	
	Hg(II)	2.7	
Simultaneous Analysis	Cd(II)	4.1	
	Pb(II)	5.0	
	Cu(II)	6.6	
	Hg(II)	5.4	
Individual Analysis	Cd(II)	4.1	5
	Pb(II)	7.2	
	Cu(II)	79.1	
	Hg(II)	6.5	
Simultaneous Analysis	Cd(II)	24.4	
	Pb(II)	5.7	
	Cu(II)	23.2	
	Hg(II)	24.6	

Cyclic voltammetry in an aqueous solution of 0.1 M KCl containing 5 mM $Fe(CN)_6^{3-}$ in the voltage range of -0.1 V to 0.6 V with scan rate varying from 10 to 100 mV s^{-1}. The results are shown in **Figure S4** in Supporting Information. It is clear that as the scan rate increases, the

anodic and cathodic peak current increases linearly (see **Figure S4a**). A plot of anodic and cathodic peak current versus scan rate is also shown in **Figure S4b**. A linear trend indicates that this process is surface confined and thus adsorption controlled process.

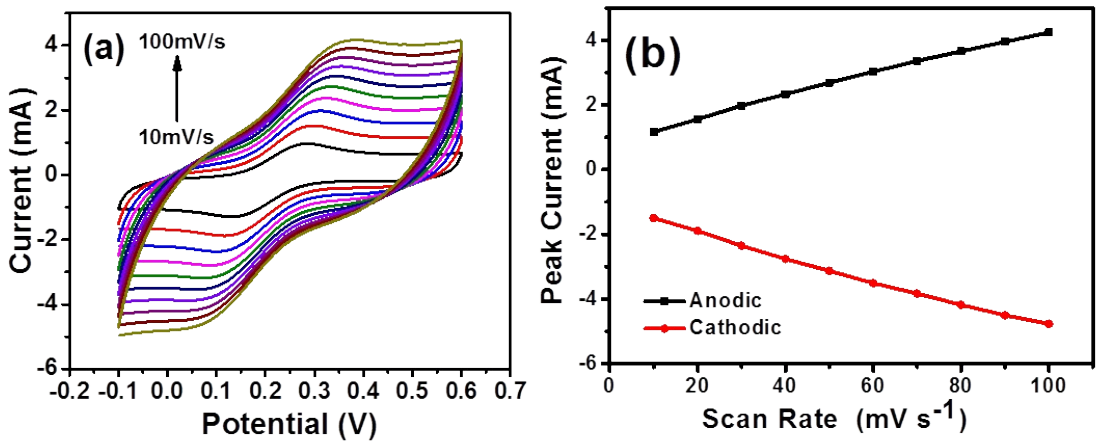

Figure S4: (a) Cyclic voltammograms at different scan rates from 10 to 100 mV s^{-1} and (b) plot of the anodic and cathodic peak current versus the scan rate.

Figure S5 shows the XPS spectra of RGO/$NiWO_4$ nanocomposite electrode after 50 CV cycles and before the stripping of heavy metals are performed. The peak positions of C 1s, O 1s, Ni 2p and W4f are similar to our nanocomposite (Figure S1). The extra peak appears in the survey scan at 685 eV corresponded to fluoride ions from the PVDF binder during the electrode preparation. In Figure S6, peaks of Cd 3d, Hg 4f, Cu 2p, and Pb 4f appeared along with C 1s, O 1s, Ni 2p and W4f, signifying the adsorption of heavy metal ions on the surface of the electrode. The peak positions after the stripping analysis are also comparable to the pristine and cycled samples.

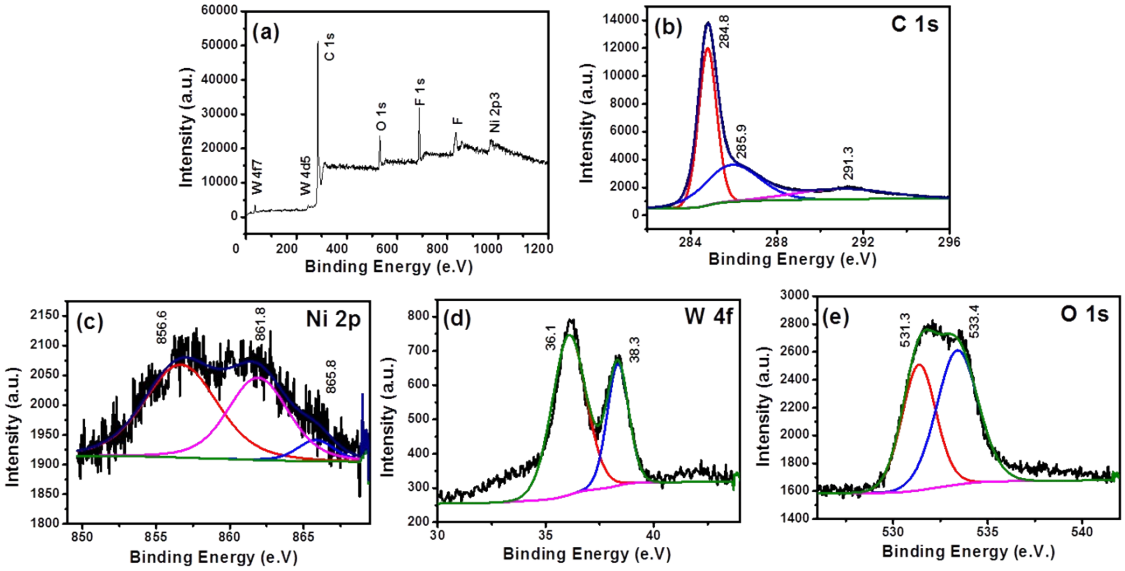

Figure S5: XPS of RGO/$NiWO_4$ nanocomposite electrode after 50 cycling but before DPASV (a) survey spectrum, (b) C 1s, (c) Ni 2p, (d) W 4f and (e) O 1s.

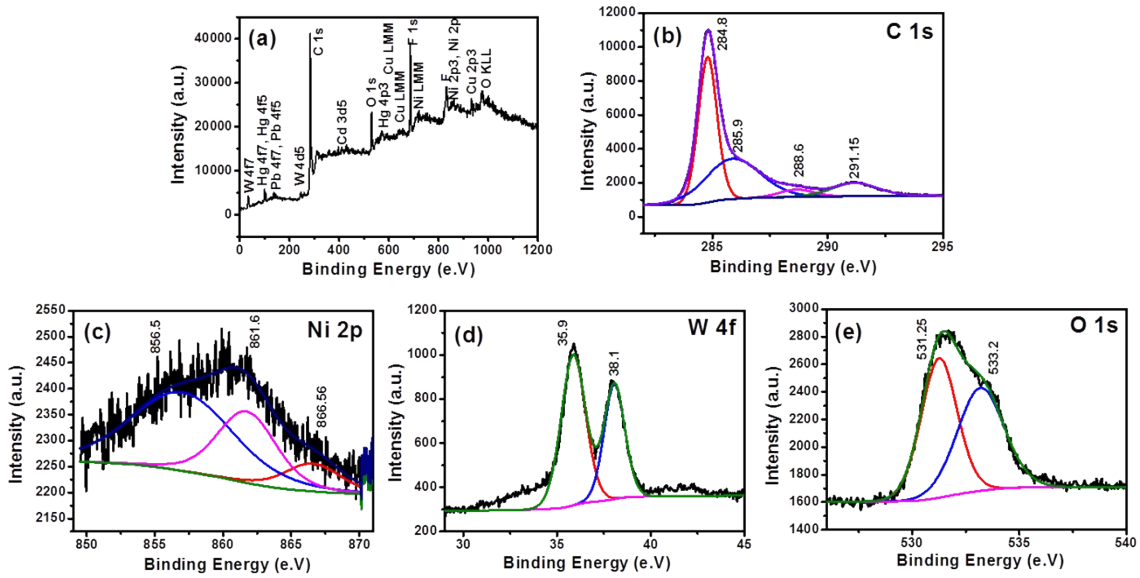

Figure S6: XPS of RGO/$NiWO_4$ nanocomposite electrode after 50 cycling and DPASV (a) survey spectrum, (b) C 1s, (c) Ni 2p, (d) W 4f and (e) O 1s.

References

1. B. P. Payne, A. P. Grosvenor, M. C. Biesinger, B. A. Kobe and N. S. McIntyre, *Surface and Interface Analysis*, 2007, **39**, 582-592.

2. M. C. Biesinger, B. P. Payne, A. P. Grosvenor, L. W. M. Lau, A. R. Gerson and R. S. C. Smart, *Applied Surface Science*, 2011, **257**, 2717-2730.
3. R. Kumar, K. Jahan, R. K. Nagarale and A. Sharma, *Industrial & Engineering Chemistry Research*, 2015, **54**, 10183-10189.
4. P. Veerakumar, V. Veeramani, S.-M. Chen, R. Madhu and S.-B. Liu, *ACS Applied Materials & Interfaces*, 2016, 8, 1319-1326.
5. R. Madhu, K. V. Sankar, S.-M. Chen and R. K. Selvan, *RSC Advances*, 2013, 4, 1225-1233.